Advances in Turbulent Flow Computations Using High-resolution Methods [1]

Dimitris Drikakis
Department of Engineering, Queen Mary, University of London,
London E1 4NS, United Kingdom,
E-mail: d.drikakis@qmul.ac.uk
and
Isaac Newton Institute for Mathematical Sciences,
University of Cambridge, United Kingdom[2]

Abstract

The paper reviews research activity in connection with the use of high-resolution methods in turbulent flow computations. High-resolution methods have proven to successfully compute a number of turbulent flows without need to resort to an explicit turbulence model. Here, we review the basic properties of these methods, present evidence from the successful implementation of these methods in turbulent flows, and discuss theoretical arguments and recent research aiming at justifying their use as an implicit turbulence model. Further, we discuss numerical issues that still need to be addressed. These include the relation of the dissipation and dispersion properties with turbulence properties such as turbulence anisotropy, as well as further validation of the methods in under-resolved simulations of near-wall turbulent attached and separated flows.

[1]The paper will also appear as an invited review article in the journal *Progress in Aerospace Sciences*, 2003.

[2]This review was written during the author's participation in the programme "Nonlinear Hyperbolic Waves in Phase Dynamics and Astrophysics" sponsored by the Isaac Newton Institute for Mathematical Sciences, University of Cambridge.

1 Introduction

In nearly every area of fluid mechanics, our understanding is inhibited by the presence of turbulence. Although many experimental and theoretical studies in the past have significantly helped to increase our physical understanding, a predictive closed theory of turbulent flows has not yet been established and is unlikely to emerge in the future. Our continuing inability to make accurate, reliable predictions seriously limits the technological advancement of aircraft and car design, turbomachinery and combustors as well as the prediction of environmental and biological flows. Hope for a universal turbulence model has been slowly replaced by the realization that the formulation of an adequate theory will continue to require a greatly improved understanding of the physics of turbulent motion. In the context of computational fluid dynamics (CFD), there are three approaches which are used to compute turbulent flows. These are the Reynolds-Averaged Navier-Stokes equations (RANS), the Large Eddy Simulation (LES) and the Direct Numerical Simulation (DNS).

The DNS approach has provided valuable information in relation to the turbulent flow structure at relatively low Reynolds numbers and for simple geometries. The use of DNS for studying unsteady flows at high Reynolds numbers ($10^5 - 10^7$) is well beyond foreseeable computing power. For example, to compute the flow around an aircraft for one second of flight time, using a supercomputer of 10^{12} Flops, it is required several thousand years and 10^{16} grid points [1]. In addition to the computing power constraints, it is not certain that DNS does indeed provide fully resolved results. To verify this, careful grid convergence studies would be required. This is not usually done in practice and one could argue that this is not feasible to be done due to inadequate computing power. Thus, RANS and LES are employed as an alternative to DNS.

In the RANS approach the equations are averaged over a time interval or across an ensemble of equivalent flows. RANS computations are extensively used in practical computations, for predicting steady-state solutions, in particular [2, 3]. Unsteadiness introduces a fundamental and profound uncertainty into the RANS approach:

Reynolds-averaging, whether ensemble or time-based, assumes that the flow is statistically steady. At the very least, the time-scale associated with the organised unsteady motion must be substantially larger than the time scale of turbulent motion (see [4, 5] for recent studies of turbulence models in unsteady aerodynamic flows). In other words, the two scales must be well separated. This condition may be satisfied in low-frequency unsteady flows but the majority of turbulent flows does not fall into this category. Closure of the phase-averaged correlations is (necessarily) identical or very similar to that adopted for the conventional averaged correlations, and this inevitably leads to models which are formally identical to their steady counterparts.

The task of RANS turbulence modelling is to provide closure relations for the Reynolds stresses by relating them to known or determinable quantities such as geometric parameters, flow scales and strains. Insight from experiments and direct simulations regarding the interactions between stresses and strains is used in RANS modelling but this approach is considered to be less universal than LES and DNS because it involves the determination of a number of unknown coefficients. Calibration of the models and estimation of the unknown coefficients are made against data from experiments and direct numerical simulations. Navier-Stokes methods have been developed aggressively in recent years for more challenging applications, and are now being used for component design and even full configurations, but mostly with "simple" eddy-viscosity models, often algebraic and at most two-equation forms. Although it is recognised that complex flows, especially those involving separation and strong vortical features, cannot be predicted adequately with such models, the emphasis on simplicity, computational speed and robustness in an industrial context militates against the adoption of more advanced models. An equally important factor has been, however, a great deal of uncertainty (indeed, confusion) on the prospect of advanced turbulence models providing adequate return for the added complexity. It is certainly true to say that the current body of knowledge arising from numerous validation studies does not provide unambiguous recommendations. In recent reviews of turbulence modelling [2, 3] the performance of a number of turbulence models, spanning from one- and two-equation linear eddy-viscosity models to more

advanced nonlinear eddy-viscosity and Reynolds-stress models, was discussed providing evidence of research into RANS turbulence modelling. Numerical accuracy is also a concern within the RANS framework. Previous research aiming to examine the effects of numerical discretisation on high-Reynolds number shock-boundary layer computations showed that the numerical accuracy depends not only on the turbulence model employed but also on the discretisation of the advective terms [6]. A recent review on the accuracy of DNS, LES and RANS computations of some shock boundary-layer interaction problems can be found in [7].

In LES the Navier-Stokes equations are filtered by convolving all dependent variables with a predefined filter in order to extract the large scale components. Then, all flow scales larger than the filter scale are computed via a modified (filtered) set of the Navier-Stokes equations while all scales smaller than the filter scale (approximately the grid size) are modelled using a subgrid scale model (SGS model). Filtering of the equations results in a system of equations, called LES equations, for the large scales. The equations also encompass unresolved correlations which are referred to as the subgrid-scale stresses (SGS stresses).

The LES equations are derived on the basis of the assumption that filtering and differentiation commute [8, 9], i.e., $\overline{\partial f/\partial x} = \partial \bar{f}/\partial x$, where the "overline" denotes the filtering operation. It can be shown [10] that the above is satisfied if the filter width is constant but not otherwise. By keeping constant the filter width, additional terms at the boundaries appear during the filtering procedure. The velocity terms vanish at solid boundaries due to the implementation of the no-slip boundary condition. However, the same does not occur for the pressure and viscous terms. To circumvent this difficulty one can use a variable filter width which separates the turbulent eddies into large-scale and small-scale eddies. The former are problem dependent whereas the latter may be modelled by a universal subgrid scale model that represents the Kolmogorov cascade at small scales, which is independent of the large scale field. Such a separation of scales may be possible away from the solid boundaries but cannot be applied close to the boundaries where turbulence manifests in the form of coherent structures which cannot be described by eddy-viscosity modelling. As a

result, the eddies close to the boundary would still need to be resolved. Application of the variable filter width will eliminate the boundary terms appearing in the filtering operation of the derivatives but the LES equations are no longer valid [10]. The commutation errors can be removed if correction terms that account for these errors are introduced in the LES equations. This will, however, raise the order of the highest derivatives in the equations and at present there are no available methods to deal with this complexity. Relevant work to the above is the derivation of special filters that can eliminate the correction terms [11, 12]. However, these filters do not satisfy positivity for the turbulent kinetic energy [10].

Other sources of error in LES arise from the discrete representation of the variables, numerical discretisation, aliasing and SGS modelling. The discrete representation has to do with the fact that in computations the variables are not continuous but are approximated on a finite basis. The errors associated with the numerical discretisation [13] arise when the differentiation operators are replaced by numerical approximations. Truncation error analysis shows that numerical discretisation leads to dissipation and dispersion terms. The dissipation terms are responsible for the numerical diffusion, especially near discontinuities, whereas the dispersion terms produce oscillations near discontinuities. In some methods, e.g., spectral schemes, spurious terms arise from the discretisation, which are responsible for the so-called "aliasing errors". These errors are manifested as numerical instabilities [14]. Further difficulties with conventional LES arise from the modelling of the SGS term; the (possible) masking of the SGS terms by the truncation error (this can possibly mitigated by using a much larger filter width than the grid size); the design of SGS models for high Reynolds number wall-bounded flows; and the quantification of the error associated with the SGS term. Concerning the last point, if DNS data are used to estimate the SGS stress, i.e., by filtering the data at a cut-off filter width and then compute the subgrid scale stresses, one finds that there are large discrepancies between these stresses and the ones computed by the model directly. Recent efforts to predict accuracy limitations in LES can be found in [15].

Over the past decade, computations using high resolution methods for turbulent

(or turbulent-like) flows have suggested that high-resolution numerical methods appear to achieve many of the properties of subgrid models, e.g., [16, 17, 18, 19, 20, 21, 22, 23, 24, 25, 26] used in LES [28, 29]. The idea to use these methods as an implicit way to numerically model turbulent flows is referred to as monotonically integrated LES (MILES) [16, 17, 19], implicit turbulence modelling [22] or embedded turbulence modelling [24, 25]. Examination of the modified equations associated with high-resolution methods as applied to the gas dynamic equations has yielded the enticing hint that characteristics implicit in these methods may mimic certain aspects of turbulence flow modelling [22].

Perhaps more importantly, these methods are often necessary to ensure a stable computation under difficult physical circumstances. Physical phenomena, associated models and their numerical solution are intertwined and should therefore be developed and solved together. In other words, the modelling and their solution cannot be separated. This approach is not generally adopted by the turbulence modelling community. Instead models are developed independently from their numerical solution, under the assumption that it is error-free. However, we may have the case where the errors are of the same differential order as the turbulence model. Further, we shall bear in mind that the accuracy in turbulent flow computations depends strongly on the numerical scheme employed to discretise the governing equations ([24, 25, 30]). Hence, even within the framework of the conventional LES where a SGS model is used, we must understand how numerical methods contribute implicitly to turbulence modelling, otherwise we may double-count the effects of turbulence through the explicit turbulence model as well as through the properties of the numerical method.

Investigation of the embedded turbulence modelling aspects of high-resolution methods may provide a fruitful avenue for understanding a number of open issues regarding computational methods and their application in multi-dimensional problems. In the following sections we will briefly review the basic properties of high resolution methods; discuss success from the implementation of the methods in turbulent flows or turbulent-like problems (e.g. Burgers' turbulence); present theoretical arguments about the relation of the methods with turbulent theories; discuss the insight one

gains from truncation error analysis and its possible connection to turbulent flow properties [22], and finally attempt to stimulate further research that will address in a more systematic framework the relation of computational methods and physics of turbulent flow.

2 Fluid flow equations

The physics of (Newtonian) fluid flow is governed by the Navier-Stokes equations. These equations can be solved by considering the coupled generalised conservation laws namely the continuity, momentum and energy equations [27]:

$$\frac{\partial \rho}{\partial t} + \nabla \cdot (\rho \mathbf{u}) = 0 \,, \tag{1}$$

$$\frac{\partial \rho \mathbf{u}}{\partial t} + \nabla \cdot (\rho \mathbf{u}\mathbf{u}) = -\nabla \cdot \mathbf{P} \,, \tag{2}$$

$$\frac{\partial e}{\partial t} + \nabla \cdot (e\mathbf{u}) = -\nabla \cdot (\mathbf{u} \cdot \mathbf{P}) - \nabla \cdot \mathbf{q} \,. \tag{3}$$

where $\mathbf{u}, \rho$, e, and $\mathbf{q}$ stand for the velocity components, density, total energy per unit volume, and heat flux, respectively. The volume forces may account for inertial forces, gravitational forces or electromagnetic forces. The tensor $\mathbf{P}$ for a Newtonian fluid is defined by

$$\mathbf{P} = p(\rho, T)\mathbf{I} + \frac{2}{3}\mu(\nabla \cdot \mathbf{u})\mathbf{I} - \mu[(\nabla \mathbf{u}) + (\nabla \mathbf{v})^{\mathbf{T}}] \tag{4}$$

where $p(\rho, T)$ is the scalar pressure, $\mathbf{I}$ is a unit diagonal tensor, T is the temperature, and μ is the dynamic viscosity coefficient. The above system is completed by an equation of state. For a perfect gas the equation of state is given by: $p = \rho RT$, where R is the gas constant.

Irrespective of the approach employed to compute turbulent flows, the equations can be cast in the conservation laws form (for a Cartesian co-ordinates system) as follows

$$\frac{\partial \bar{\mathbf{U}}}{\partial t} + \frac{\partial \bar{\mathbf{E}}(\bar{\mathbf{U}})}{\partial x} + \frac{\partial \bar{\mathbf{F}}(\bar{\mathbf{U}})}{\partial y} + \frac{\partial \bar{\mathbf{G}}(\bar{\mathbf{U}})}{\partial z} = \mathbf{S}(\bar{\mathbf{U}}) \ , \tag{5}$$

where $\bar{\mathbf{U}}$ is the array of flow variables; $\bar{\mathbf{E}}(\bar{\mathbf{U}})$, $\bar{\mathbf{F}}(\bar{\mathbf{U}})$ and $\bar{\mathbf{G}}(\bar{\mathbf{U}})$ are the fluxes in x, y and z directions, respectively. The "bar" denotes filtering and averaging for the LES and RANS approach, respectively; in the case of DNS there will be no "bar" over the fluxes. The term $\mathbf{S}(\bar{\mathbf{U}})$ on the right-hand-side of (5) contains the viscous terms, as well as the SGS and Reynolds stresses for the case of LES or RANS, respectively. For $\mathbf{S}(\bar{\mathbf{U}}) = 0$ we obtain a system of hyperbolic conservation laws. The nonlinear terms are contained in the fluxes on the left-hand-side of (5). During the last four decades, there have been intensive research efforts to develop accurate methods for solving hyperbolic conservation laws. The development of high-resolution methods for solving the inviscid equations of gas dynamics has received most of the attention. The use of these methods for computing turbulent flows has also attracted research interest over the past decade. In the next section we review the basic properties of these methods before we discuss their implementation in turbulent flows. For an introductory review of high-resolution methods for the solution of compressible Euler equations we refer the reader to [31]. A review on the development and implementation of the methods in incompressible flows can be found in [32].

3 High-resolution methods

We classify as high-resolution methods those with the following properties [33]:

- Provide at least second order of accuracy in smooth areas of the flow.
- Produce numerical solutions (relatively) free from spurious oscillations.
- In the case of discontinuities, the number of grid points in the transition zone containing the shock wave is smaller in comparison with that of first-order monotone methods.

The motivation for the development of high-resolution methods emerges from our effort to circumvent Godunov's theorem [35] that states: *There are no monotone, linear schemes for the linear advection equation of second or higher order of accuracy.* In other words, second-order accuracy and monotonicity are contradictory requirements. The key to circumvent Godunov's theorem lies on the assumption made in the theorem that the schemes are linear. Therefore, if we want to design methods which provide at least second order of accuracy and at the same time avoid spurious oscillations in the vicinity of large gradients, then we need to develop nonlinear methods. The development of high-resolution methods is done in the one-dimensional context due to the lack of adequate theory in multi-dimensions. Even though a numerical scheme can be designed to be second-order accurate for one-dimensional problems its accuracy in multiple dimensions is not guaranteed to be second-order. This has been proven [36] by various numerical experiments using well known second-order methods.

3.1 Properties of high-resolution methods

To discuss properties of numerical methods it is convenient to consider the one-dimensional counterpart of (5) without source terms

$$\frac{\partial \mathbf{U}}{\partial t} + \frac{\partial \mathbf{E}(\mathbf{U})}{\partial x} = 0 \ . \tag{6}$$

One can discuss numerical approximations to weak solutions w_i which can be obtained, for example, by $(2k+1)$-point explicit schemes in conservation form[3]

$$w_i^{n+1} = w_i^n - \frac{\Delta t}{\Delta x}(\tilde{\mathbf{E}}_{i+1/2}^n - \tilde{\mathbf{E}}_{i-1/2}^n) \ , \tag{7}$$

where for the numerical flux $\tilde{\mathbf{E}}$ yields $\tilde{\mathbf{E}}_{i+1/2}^n = \tilde{\mathbf{E}}(w_{i-k+1}^n, ..., w_{i+k}^n)$, and n denotes the time level. The numerical flux should also be consistent with the flux $\mathbf{E}$, i.e., $\tilde{\mathbf{E}}(\mathbf{U}, ..., \mathbf{U}) = \mathbf{E}(\mathbf{U})$.

[3]Throughout the paper i denotes cell centered value and $i + 1/2$ denotes intercell value.

Weak solutions of (6) should satisfy the inequality $\tilde{\mathbf{U}}_t + \mathcal{F}_x \leq 0$ (entropy condition), where $\tilde{\mathbf{U}}$ is a convex function of $\mathbf{U}$, i.e. $\tilde{\mathbf{U}}_{\mathbf{UU}} > 0$, and $\tilde{\mathbf{U}}$ satisfies $\tilde{\mathbf{U}}_{\mathbf{U}}\mathbf{E}_{\mathbf{U}} = \mathcal{F}_{\mathbf{U}}$, where $\mathcal{F}$ is the entropy flux [33]. The solution (7) converges to a weak solution of (6) when the following conditions are satisfied:

1. The total variation of the solution (defined below) with respect to x is uniformly bounded with respect to t, Δt and Δx.

2. The scheme (7) satisfies the entropy condition.

3. The entropy condition implies unique solution of the initial value problem.

Conditions 1 and 2 can be satisfied by the addition of artificial viscosity to the numerical scheme. This will possibly provide non-oscillatory solutions at the expense of loss of physical information thus deteriorating the overall computational accuracy.

Below we review some of the basic properties that are considered in the design of high-resolution schemes. The total variation of a function $u(x)$ is defined as

$$\mathrm{TV(u)} = \lim_{\epsilon \to 0} \sup \frac{1}{\epsilon} \int_{-\infty}^{+\infty} |\mathrm{u(x+\epsilon) - u(x)}| \, \mathrm{dx} \, . \tag{8}$$

If $u(x)$ is smooth then (8) can be written

$$\mathrm{TV(u)} = \int_{-\infty}^{+\infty} |\mathrm{u'(x)}| \, \mathrm{dx} \, . \tag{9}$$

If u is a function of space and time, $u(x,t)$, then we define the total variation of u at fixed time, t. In a discretised domain, u is a function of the mesh and its total variation at a time instant indicated by the index n is defined as

$$\mathrm{TV(u^n)} \equiv \mathrm{TV(u(t))} = \sum_{\mathrm{i}=-\infty}^{+\infty} |\mathrm{u_{i+1}^n - u_i^n}| \, . \tag{10}$$

The function u is assumed to be either 0 or constant as the index i approaches infinity, in order to obtain finite total variation.

The monotonicity property is defined for a scalar conservation law

$$\frac{\partial u}{\partial t} + \frac{\partial f(u)}{\partial x} = \frac{\partial u}{\partial t} + \alpha(u)\frac{\partial u}{\partial x} = 0 \ , \tag{11}$$

where $\alpha(u) = \mathrm{d}f/\mathrm{d}u$, $u(x,0) = \phi(x)$, $-\infty < x < \infty$, and $\phi(x)$ is assumed to be of bounded total variation.

An important property of the weak solution of the scalar initial value problem is the *monotonicity property* according to which:

- No new local extrema in x may be created.
- The value of a local minimum increases, i.e., it is a nondecreasing function [33], and the value of a local maximum decreases, i.e., it is a nonincreasing function [33].

Thus the total variation, TV(u(t)), is a decreasing function of time

$$\mathrm{TV(u(t_2))} \leq \mathrm{TV(u(t_1))} \quad \forall \quad \mathrm{t_2} \geq \mathrm{t_1} \ . \tag{12}$$

The explicit scheme of (7) can also be written in a shorter form as

$$w_i^{n+1} = H(w_{i-k}^n, w_{i-k+1}^n, ..., w_{i+k}^n) = L \cdot w_i^n \ , \tag{13}$$

where L is an operator. We say that the scheme (13) is *total variation nonincreasing* (TVNI) if for all w

$$\mathrm{TV(L \cdot w)} \leq \mathrm{TV(w)} \ . \tag{14}$$

The scheme (13) is monotonicity preserving if the finite difference operator L is monotonicity preserving, that is, if w is a monotone mesh function, so is $L \cdot w$. Moreover, the scheme (13) is a monotone scheme if H is a monotone increasing function of each of its $2k + 1$ arguments. The hierarchy of these properties can be stated as follows: the set of monotone schemes is contained in the set of TVD schemes and this is in turn contained in the set of monotonicity preserving schemes.

Monotone schemes can be constructed as upwind or centered. TVD and Essentially Non-Oscillatory (ENO) [34] schemes can also be designed to be monotone in the one-dimensional context. However, the set of monotone schemes is the smallest set of schemes and is a subset of the set of TVD schemes.

For a constant coefficient $\alpha(u) = \alpha$, we obtain the linear advection equation. Well known schemes such as the Godunov first-order upwind scheme [35] and the Lax-Wendroff scheme [37], among others, can cast in the general form

$$w_i^{n+1} = \sum_{l=-k_L}^{l=k_R} b_l w_{i+l}^n \ , \tag{15}$$

where k_L and k_R are two non-negative integers and b_l are constant coefficients. Harten [33] has shown that the linear finite difference approximation (15) is monotonicity preserving if the coefficients b_l are non-negative, i.e., $b_l \geq 0 \ , \quad -k_L \leq l \leq k_R$.
Thus any linear monotonicity preserving scheme is a monotone, first-order, accurate scheme.

3.2 Limiters

Limiters are the general nonlinear mechanism that distinguishes modern methods from classical linear schemes. These are sometimes referred to as flux limiters or slope limiters, but their role is similar: to act as a nonlinear switch between more than one underlying linear methods thus adapting the choice of numerical method based upon the behavior of the local solution. The general practice is to base the analysis of the nonlinear method on the linear analysis of the available methods to be chosen by the limiter. The limiter can also be included in the analysis providing a nonlinear truncation error analysis even when the equation being solved is linear. Limiters result in nonlinear methods even for linear equations in order to achieve second-order accuracy simultaneously with monotonicity.

Second-order accurate three- and five-point (nonlinear) schemes of the form (13) can be rewritten in the form [33]

$$w_{i+1}^n = w_i^n - C_{i-1/2}\Delta w_{i-1/2} + D_{i+1/2}\Delta w_{i+1/2} \ , \tag{16}$$

where $\Delta w_{i+1/2} = w_{i+1}^n - w_i^n$ and

$$\left.\begin{array}{rcl} C_{i-1/2} & \equiv & C(w_{i-2}, w_{i-1}, w_i, w_{i+1}) \\ D_{i+1/2} & \equiv & D(w_{i-1}, w_i, w_{i+1}, w_{i+2}) \end{array}\right\} \ . \tag{17}$$

Harten [33] has proved that any scheme (17) satisfying the inequalities

$$\left.\begin{array}{l} C_{i+1/2} \geq 0 \quad , \quad D_{i+1/2} \geq 0 \\ 0 \leq C_{i+1/2} + D_{i+1/2} \leq 1 \end{array}\right\} \ , \tag{18}$$

is a TVNI scheme. This is also referred to as *Harten's theorem*. Harten's theorem can be used to construct flux limiters.

An alternative criterion to Harten's theorem is the data compatibility condition as proposed by Roe [38, 39] (see [31] for details). Roe's idea was to circumvent Godunov's theorem by constructing adaptive algorithms that would adjust themselves to the local nature of the solution. This leads to the design of schemes with variable coefficients (which are functions of the data), i.e., in nonlinear schemes even for linear PDEs such as the linear advection equation. A scheme is compatible if the solution w_{i+1}^n at each point i is bounded by the pair (w_{i-s}^n, w_i^n), where $s \equiv \text{sign}(\alpha)$ [31]. The data compatibility condition is satisfied by the inequality

$$0 \leq \frac{w_i^{n+1} - w_i^n}{w_{i-s}^{n+1} - w_i^n} \leq 1 \ . \tag{19}$$

By applying the data compatibility condition for specific sets of data, we can construct combination of schemes which satisfy the whole set of data. This would eventually result in adaptive, nonlinear schemes that are monotone and second order accurate. Further contributions to design flux limiters for high-resolution methods can be found in [40, 41, 42]. The MUSCL approach [43, 44, 45, 46, 47, 48] also allows the construction of high-resolution methods. Nonlinear versions of these schemes that

"avoid" spurious oscillations can be constructed by limiting the slopes in the original MUSCL scheme according to some TVD constraints (for a review see [31, 49]).

Other definitions that are sometimes used to design advective schemes is that for positive schemes [51] and the "universal" limiter [52]. The approach based on positive schemes allows different time stepping schemes to be used by treating the space and time discretisation separately [51]. Thuburn [50] has shown that different approaches for constructing limiters can lead to equivalent schemes at least in the context of the one-dimensional linear advection equation. However, the differences between the aforementioned approaches still remain important since each of these approaches can be extended and utilised in different ways, for example, the TVD approach can be extended to conservation laws other than the advection equation.

Numerical flux limiters can act like a dynamic, self-adjusting models, modifying the numerical viscosity to produce a nonlinear eddy viscosity. The limiters can be cast in a differential form resulting from their modified equations [53]. In the case of a sign-preserving limiter, the form is $1 - c\Delta x\,|w_x/w|$ and for a monotone (minmod) limiter it $1 - c\Delta x\,|w_{xx}/w_x|$ (c is a constant) [25]. The sign-preserving limiter produces a form for the viscosity that is similar to Smagorinsky's nonlinear viscosity [54]. With a small amount of reinterpretation, a broad class of modern numerical methods can be viewed as dynamic mixed LES models.

Limiters are used in the data reconstruction step, where data cell average values are replaced by piece-wise linear functions in each cell $[x_{i-1/2}, x_{i+1/2}]$, e.g.

$$w_i(x) = w_i^n + \frac{x - x_i}{\Delta x}\Delta_i \ , \tag{20}$$

where Δ_i is a chosen slope defined by differences of u values. Examples of some limiters are given below. Van Leer [43, 44, 45, 46] proposed the MUSCL approach to replace the piece-wise constant data in the first-order Godunov method, as a first step to achieve high-order of accuracy. In the MUSCL approach, the slopes Δ_i are defined by

$$\Delta_i = \frac{1}{2}(1+k)\Delta w_{i-1/2} + \frac{1}{2}(1-k)\Delta w_{i+1/2} \tag{21}$$

where

$$\Delta w_{i-1/2} = w_i^n - w_{i-1}^n \, , \Delta w_{i+1/2} = w_{i+1}^n - w_i^n \, , \tag{22}$$

and k is a parameter that can take values in the interval $[-1, 1]$. The MUSCL approach allows the construction of high-order methods but spurious oscillations will still be present in the vicinity of large gradients thus violating the requirement for a TVD scheme. To circumvent this difficulty nonlinear versions of the MUSCL (or MUSCL-type) schemes can be constructed by replacing the slopes Δ_i by limited slopes $\overline{\Delta}_i$ according to some TVD constraints. For example, limited slopes can be obtained [55] by

$$\overline{\Delta}_i = \begin{cases} \max[0, \min(\omega\Delta_{\mathrm{i}-1/2}, \Delta_{\mathrm{i}+1/2}), \min(\Delta_{\mathrm{i}-1/2}, \omega\Delta_{\mathrm{i}+1/2})] & \text{for} \quad \Delta_{i+1/2} > 0 \\ \min[0, \max(\omega\Delta_{\mathrm{i}-1/2}, \Delta_{\mathrm{i}+1/2}), \max(\Delta_{\mathrm{i}-1/2}, \omega\Delta_{\mathrm{i}+1/2})] & \text{for} \quad \Delta_{i+1/2} < 0 \end{cases} \tag{23}$$

where $\omega = 1$ and 2 give the MINMOD and SUPERBEE flux limiters, respectively.

The construction of limiters does make sense not only for compressible flows that encompass discontinuities, but also for incompressible flows where large gradients, e.g. due to the appearance of vortices and turbulence, occur [24]. Limiters play an essential role in the effective dissipation of a scheme as well as acting as a trigger for a dynamic dissipative scheme.

In dynamic LES models [56, 57] the viscosity is adjusted locally based on whether the flow exhibits a similar structure at adjacent length scales. There is an implicit correspondence between some limiter forms to the dynamic SGS models in LES. Further, the limiters provide additional utility by comparing several local estimates of a derivative. If these estimates are close enough in magnitude, the flow is treated as being resolved, allowing the method to detect smooth (laminar) flow.

One can also produce a limiter of lower differential order that preserves the sign of the data rather than monotonicity [25]. Such limiter forms can be derived for the multidimensional positive definite advection transport algorithms (e.g. [58]) using the modified equations analysis [22, 58], as well as for TVD Godunov-type schemes applicable to incompressible flows [24] .

3.3 Nature of algorithmic components

To fully assess the similarities of high-resolution methods with turbulence models for LES, we will focus on the numerical intercell flux, $\tilde{\mathbf{E}}_{i+1/2}$, of a Godunov-type method

$$\tilde{\mathbf{E}}_{i+1/2} = \frac{1}{2}(\mathbf{E}_L + \mathbf{E}_R) - \frac{1}{2}\left|\mathbf{A}\right|(\mathbf{U}_R - \mathbf{U}_L) \ , \tag{24}$$

where L and R denote the left and right states in the Riemann solution, and $\mathbf{A}$ is the flux Jacobian. The absolute value of A can be found via an eigen-decomposition, $\mathbf{A} = \mathcal{R}|\Lambda|\mathcal{L}$, where $\mathcal{R}$, Λ and $\mathcal{L}$ are the right eigenvectors, eigenvalues and left eigenvectors of A, respectively. This is a fairly generic and standard manner to introduce upwinding into a numerical method [31]. The left and right states can be accessed via interpolation from cell centres to the edges. This is the reconstruction step of a high resolution method. The interpolation is usually limited by using limiters that have the numerical properties discussed in the preceding section.

In the case of TVD methods the intercell flux is given by

$$\tilde{\mathbf{E}}_{i+1/2} = \frac{1}{2}(\mathbf{E}_L + \mathbf{E}_R) - \frac{1}{2}|\mathbf{A}|(1-\psi)(\mathbf{U}_R - \mathbf{U}_L) \ , \tag{25}$$

where ψ is a limiter. An alternative formulation is to write the flux as a combination of low and high order fluxes

$$\tilde{\mathbf{E}}_{i+1/2} = \tilde{\mathbf{E}}^{\text{low}}_{i+1/2} + \phi(\tilde{\mathbf{E}}^{\text{high}}_{i+1/2} - \tilde{\mathbf{E}}^{\text{low}}_{i+1/2}) \tag{26}$$

where ϕ is a limiter, $\tilde{\mathbf{E}}^{\text{low}}$ is a first-order flux, e.g., the first-order Godunov [35] or Lax-Friedrichs flux [59] among others, and $\tilde{\mathbf{E}}^{\text{high}}$ is a high-order, at least second-order,

flux, e.g., the Lax-Wendroff flux [37].[4]

According to (24), the flux can be generally decomposed into terms that are hyperbolic and dissipative in nature. We can use this effective decomposition to identify what the physical effect of various algorithmic components are. The portion that is the sum of the local contributions (the mean flux) is hyperbolic, while those proportional to the difference in the variables is dissipative with a magnitude proportional to the coefficient of numerical viscosity. The TVD flux (25) can also be viewed in a similar way: the flux is a second-order centered flux with a dissipative term that yields first-order upwinding that is triggered by a limiter. Thus, in the case of TVD methods the action of the high resolution scheme is entirely dependent upon the limiter acting on the numerical viscosity.

Insight into the nature of algorithmic components and its relation to the flow physics can also be obtained by nonlinear truncation error analysis. Let us consider, for example, the nonlinear truncation error arising from the discretization of the following equation [25]

$$\frac{\partial \mathbf{U}}{\partial t} + \frac{\partial \mathbf{E}(\mathbf{U})}{\partial x} = 0 \rightarrow \frac{\partial \mathbf{U}}{\partial t} + \frac{\partial \mathbf{E}(\mathbf{U})}{\partial \mathbf{U}} \frac{\partial \mathbf{U}}{\partial x} = 0 \; . \tag{27}$$

Using a first-order upwind scheme including the leading order (spatial) truncation error, we obtain the modified equation

$$\begin{aligned} \frac{\Delta \tilde{\mathbf{U}}}{\Delta t} \; + \; & \mathbf{A}(\tilde{\mathbf{U}}) \frac{\Delta \tilde{\mathbf{U}}}{\Delta x} = \\ & \frac{\Delta x}{2} \left[\left| \frac{\partial \hat{\mathbf{E}}\left(\hat{\mathbf{U}}\right)}{\partial \hat{\mathbf{U}}} \right| \frac{\partial^2 \hat{\mathbf{U}}}{\partial x^2} + \text{sign}\left(\frac{\partial \hat{\mathbf{E}}\left(\hat{\mathbf{U}}\right)}{\partial \hat{\mathbf{U}}} \right) \frac{\partial^2 \hat{\mathbf{E}}\left(\hat{\mathbf{U}}\right)}{\partial \hat{\mathbf{U}}^2} \left(\frac{\partial \hat{\mathbf{U}}}{\partial x} \right)^2 \right] \; , \end{aligned} \tag{28}$$

where the left-hand-side of the above equation contains the terms arising from the discretisation of the differential equation. The term $\hat{\mathbf{E}}$ is the flux calculated by using the solution $\hat{\mathbf{U}}$ of the modified equation. The first term on the right-hand-side is the second-order dissipation most commonly associated with this method whereas

[4] A review of TVD formulations for compressible and incompressible flow equations can be found in [31, 49] and [32], respectively.

the second term is primarily dispersive in character and produces oscillations near discontinuities.

In the case of Lax-Wendroff [37] scheme

$$\frac{\Delta\tilde{\mathbf{U}}}{\Delta t}+\mathbf{A}(\tilde{\mathbf{U}})\frac{\Delta\tilde{\mathbf{U}}}{\Delta x}= \tag{29}$$
$$\Delta x^2\left[-\frac{1}{6}\frac{\partial\hat{\mathbf{E}}\left(\hat{\mathbf{U}}\right)}{\partial\hat{\mathbf{U}}}\frac{\partial^3\hat{\mathbf{U}}}{\partial x^3}-\frac{1}{2}\frac{\partial^2\hat{\mathbf{E}}\left(\hat{\mathbf{U}}\right)}{\partial\hat{\mathbf{U}}^2}\frac{\partial\hat{\mathbf{U}}}{\partial x}\frac{\partial^2\hat{\mathbf{U}}}{\partial x^2}-\frac{1}{6}\frac{\partial^3\hat{\mathbf{E}}\left(\hat{\mathbf{U}}\right)}{\partial\hat{\mathbf{U}}^3}\left(\frac{\partial\hat{\mathbf{U}}}{\partial x}\right)^3\right]$$

The terms on the right-hand-side have mixed effect although it is dominated by dispersive effects. By using a limiter to hybridize the upwind and Lax-Wendroff method we can accentuate the dissipative effects seen in the leading order spatial truncation error. Limiters will be seen to introduce standard sorts of nonlinear eddy viscosities through the numerical flux. If the limiters are not active, the dissipative term will vanish and in the case of second-order methods a fourth-order dissipation will result.

Margolin and Rider [22] have used truncation error analysis (modified equation), accompanied by numerical experiments for the Burgers' equation, to show that the truncation error terms of high-resolution schemes (their analysis was applied to MP-DATA scheme [58]) have physical significance and are the corrections necessary to represent the evolution of a finite volume of fluid. They expanded the velocity in a Taylor series and averaged the equations over those length and time scales thus leading to several new terms that scaled with the square of the space or of the time intervals. For "non-smooth" flows[5] in (e.g. turbulence) for which the fluid velocity is not smooth over particular length and time scales, they assumed that the averaged velocity is smooth at least over these scales. With this assumption, they were able to show that the same averaged equations that govern the evolution of laminar flows also govern turbulent flows.

In the past, Hirt [60], among others, has investigated the nature of errors in finite

[5]By "non-smooth" we do not mean that the flow variables are discontinuous variables in a strict mathematical sense, e.g., like shock waves, but their variation encompass (very) steep gradients.

difference algorithms. Hirt's work is one of the early attempts to give a physical meaning to numerical errors, e.g., the notion that even and odd order errors are associated with diffusion and dispersion processes, respectively. This notion led later to the proof of entropy satisfying solutions in connection with upstream differencing [61]. Recent work on the analysis of nonlinear methods and equations using modified equations can be found in [26, 62]. The ultimate judgement on the ability of high-resolution methods to compute turbulent flows will be made on the basis of the results obtained for different flow problems. Computational evidence from the implementation of the methods in a variety of flow problems is discussed in the next section.

4 Computational evidence

The success of high-resolution methods in computing turbulent flows without using SGS models has also been demonstrated by a number of simulations presented in the literature: forced and decaying homogeneous isotropic turbulence, [18, 19, 63, 64]; subsonic and supersonic jet flows [65, 66, 67]; fully turbulent channel flows and flows over backward facing steps [68]; transitional jet flows [19]; homogeneous compressible turbulence [69, 70, 71]; pulsatile flows in three-dimensional stenotic pipes pertinent to biological flows [72, 73]; chemically reactive flows [16, 74]; mixing layers [77]; and a variety of low and high speed flows [75].

In this section we present numerical evidence from the implementation of high-resolution methods to resolve turbulent flows without need to resort to a SGS model. For comparison purposes, we also include examples using an explicit turbulence model.

4.1 Burgers' turbulence

As a first example we examine the behavior of high resolution methods with and without SGS models for simulations of Burgers' turbulence [76]. The Burgers' equation can be considered as the one-dimensional analog of the Navier-Stokes equations.

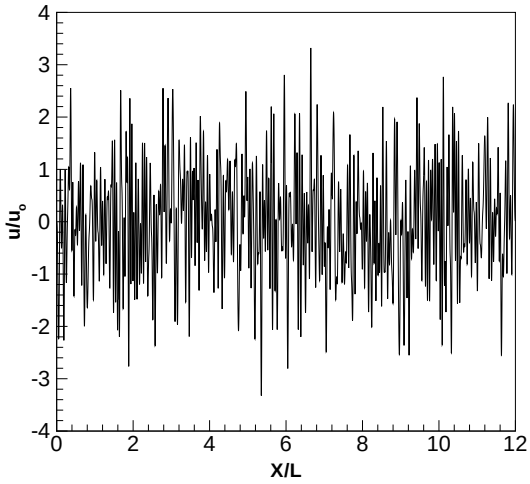

Figure 1: Velocity profile considered as initial condition in the simulations of Burgers' turbulence. Results from [24]: *"Embedded turbulence model in numerical methods for hyperbolic conservation laws"*, by D. Drikakis, Copyright 2002. ©John Wiley & Sons Limited. Reproduced with permission.

The problem of Burgers' turbulence is described by $\partial u/\partial t + u\ \partial u/\partial x = \nu\ \partial^2 u/\partial x^2$, subject to periodic boundary conditions $u(x,t) = u(x+l,t)$, $0 \leq x \leq l$, and a random initial condition for the velocity u (Fig. 1).

The random initial condition of Fig. 1 exhibits maximum value of the wave spectrum at $\log(k) = 1.283$ [24]. The velocity has become dimensionless by defining a characteristic length scale $L_o = 1/\log^{-1}(1.283)L = 0.052L$ (where L is an arbitrary unit of length; here $L = 1$), and a characteristic velocity u_o as the root mean square of the initial condition. The viscosity ν can then be defined by $\nu = (L_o u_o)/Re$, where Re is the Reynolds number. We have conducted simulations for $Re = 6,000$ in a domain of length $l = 12L = 12$, using a very fine grid (9,000 grid points) and a very small time step ($\Delta t = 0.0001$) [24]. The obtained solution (henceforth labeled DNS) is grid and time-step independent and can thereby be considered as the "exact" solution.

In [24] coarsely-resolved simulations have been carried out on a 700×100 space-time grid using different numerical schemes with and without different SGS models

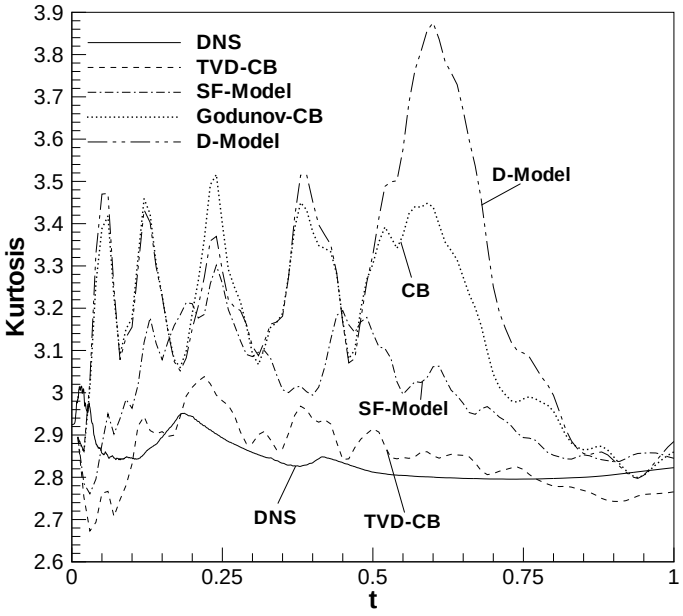

Figure 2: Kurtosis distribution for simulation of Burgers' turbulence using characteristic-based (CB) and TVD schemes (TVD-CB) with and without SGS scale models. Results from [24]: *"Embedded turbulence model in numerical methods for hyperbolic conservation laws"*, by D. Drikakis, Copyright 2002. ©John Wiley & Sons Limited. Reproduced with permission.

[24]. The following numerical variants have been employed: i) the characteristic-based (Godunov-CB) scheme of [77] without a SGS model; ii) the TVD-CB scheme of [24] without a SGS model; iii) the CB scheme in conjunction with the modified version of the dynamic SGS model [56] – the solution is labeled as "D-Model"; iv) the CB scheme in conjunction with the structure-function SGS model [78] – the solution is labeled as "SF-Model". The results for the kurtosis distribution Fig. 2 reveal that: i) modelling the unresolved scales through a SGS model does not always improve the results; for example, compare the Godunov-CB solutions with and without the dynamic model; ii) high resolution schemes designed to satisfy the total variation diminishing (TVD)

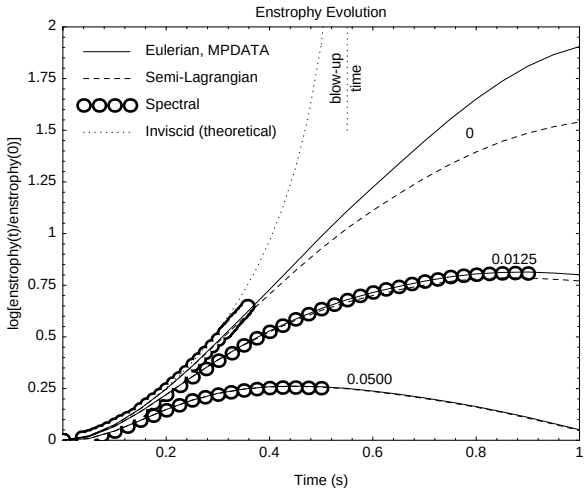

Figure 3: Results from [79] for the decaying turbulence of a homogeneous incompressible fluid in a triply-periodic cube. Solid lines are simulation results using the high-resolution scheme MPDATA [58] without an explicit SGS model; dashed lines are for semi-Lagrangian simulations; circles are the results of Herring and Kerr [81] and dotted lines are a theoretical estimate of inviscid flow (see text for details). Reproduced with kind permission of Kluwer Academic Publishers, book *"Turbulent Flow Computation"*, 2002, Chapter 8 (pp. 279-312), "Forward-in-time differencing for fluids: Simulation of geophysical turbulence", by P.K. Smolarkiewicz and J.M. Prusa, Fig. 8.3 (page 290), D. Drikakis & B.J. Geurts (eds.), ©2002, Kluwer Academic Publishers (printed in the Netherlands) [79].

condition can significantly improve the predictions without even using a SGS. Comparison of the average kurtosis value for the various computations including the case where the TVD-CB scheme is used in conjunction with the structure-function SGS model have shown that the computation based upon the TVD-CB scheme without a SGS model gives the closest agreement with the DNS solution [24].

4.2 Decaying turbulence of a homogeneous incompressible fluid

The second example is from simulations of Smolarkiewicz and Prusa [79] (see also [80] for further discussion) for the decaying turbulence of a homogeneous incompressible fluid in a triply-periodic cube; a canonical problem in turbulence studies. Due to the assumed homogeneity of the thermodynamics, and the lack of near-wall effects, the focus of the problem is on the nonlinearity of the convective derivatives $\mathbf{u}\nabla\mathbf{u}$ in the momentum equation. In [79] the simulations were carried out using the nonoscillatory forward in time (NFT) advection scheme MPDATA [58].

Figure 3 displays the numerical results for the evolution of enstrophy for three values of viscosity, $\nu = 0.0500$, $\nu = 0.0125$, and $\nu = 0$ $m^2 s^{-1}$ (as indicated in Fig. 3). Simulations with MPDATA (and the nonoscillatory semi-Lagrangian option of this model) follow precisely the 256^3 pseudo-spectral simulations of Herring and Kerr [81]. Solid lines are for MPDATA experiments and dashed lines for semi-Lagrangian experiments, whereas Herring-Kerr results are marked with circles. In the same figure a theoretical estimate for inviscid flow (dotted lines)—based upon the elementary enstrophy relationship for 3D isotropic turbulence and a phenomenological model for skewness (with free parameters evaluated by matching the numerical results at small time when viscous effects are negligible); see also Chapter VI.7 in [82].

There is an excellent agreement of the MPDATA and pseudo-spectral calculations for DNS ($\nu > 0$). Firstly, the results show that the MPDATA model (a finite volume high-resolution method) is at least as accurate as the pseudo-spectral method. Secondly, the results also reveal that without viscous dissipation ($\nu = 0$), unlimited enstrophy growth is predicted. Herring and Kerr [81] note that with rapid enstrophy growth, the spectral calculations become computationally unstable and must be terminated after ~ 0.35s. Up to this time, the MPDATA, spectral, and theoretical results agree closely. After the collapse of the spectral model, the MPDATA computations continue to provide a stable solution but there are discrepancies with the theoretical estimate. As the authors explain, this divergence is due to the flow topol-

ogy condition being enforced by the MPDATA scheme (e.g., an embedded SGS model develops). Essentially, enstrophy has increased to the point where velocity gradients are so large that the local derivatives should be limited to obtain stability of the computations. The results of Fig. 3 suggest that the net effect of this limiting is that the MPDATA scheme results in an effective viscosity (of $\sim 0.004\ m^2 s^{-1}$for the Eulerian computation and approximately double that for the MPDATA semi-Lagrangian computation [79]). In a sense, high-resolution schemes may be considered as producing the most stable LES result for an inviscid flow at a given computational resolution.

4.3 Convective planetary boundary layer

In previous studies, Smolarkiewicz and Prusa [79], as well as Margolin et al. [23], demonstrated that an atmospheric code based on MPDATA [58] can accurately reproduce (i.e., in close agreement with field/laboratory data and the existing benchmark computations) the structure of the convective planetary boundary layer. They carried out simulations with and without an explicit SGS turbulence model (see [79] for details of the SGS model). Their results showed that when an explicit turbulence model was implemented, MPDATA did not add any unnecessary diffusion. When no explicit turbulence scheme was employed, the high-resolution method itself appeared to include an effective SGS model. They also reported that using the explicit turbulence model with the eddy viscosity reduced by some factor, MPDATA added just enough dissipation. These numerical experiments demonstrate the self-adaptive character of the high-resolution method and suggest the physically realistic character of its truncation error (i.e. numerical dissipation).

Figure 4 shows results for the resolved heat flux $\langle T'w' \rangle$ (normalized appropriately), where T and w are the temperature and vertical velocity, respectively, and primes denote deviation from the horizontal average $< \cdot\cdot >$ [79, 23]. The three curves shown in the figure represent mean profiles from three different simulations: the short-dashed curve is from LES benchmark simulations of Schmidt and Schumann [83] using a centred numerical scheme both in space and in time; the long-dashed curve is from

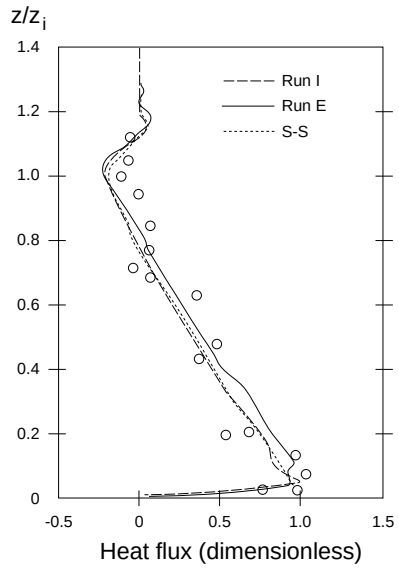

Figure 4: Simulation results for the convective atmospheric boundary layer using an explicit SGS model (Run I) and without an explicit SGS model (Run E). The short dashed curve (S-S) are the results from [83]. Reproduced with kind permission of Kluwer Academic Publishers, book *"Turbulent Flow Computation"*, 2002, Chapter 8 (pp. 279-312), "Forward-in-time differencing for fluids: Simulation of geophysical turbulence", by P.K. Smolarkiewicz and J.M. Prusa, Fig. 8.6 (page 294), D. Drikakis & B.J. Geurts (eds.), ©2002, Kluwer Academic Publishers (printed in the Netherlands) [79].

LES simulations with MPDATA, and the solid curve is for MPDATA with no explicit subgrid-scale model; circles represent field and laboratory data. The comparability of all the results with the data is excellent (for other characteristics of the flow, see [79]).

The most important result in Figure 4 is the the accuracy of the high-resolution method in LES without need to resort to a SGS model. In contrast to linear methods, the success of high-resolution methods in turbulent flows is due to the self-adaptiveness of these schemes during the simulation. When the explicit SGS model is included the resolved flow is sufficiently smooth, and the part of the numerical

algorithm that assures high-resolution properties is essentially switched off. When no explicit SGS model is used the high-resolution scheme adapts the numerics assuring solutions that are apparently as smooth as those generated with explicit SGS models. One should bear in mind that the dissipation of high-resolution methods cannot be universally quantified since the advective scheme can be effectively either non-dissipative or dissipative, depending upon the presence or absence, respectively, of an explicit SGS model [79].

However, the limits of the embedded turbulence modelling approach in the context of under-resolved simulations, for wall-bounded flows in particular, need to be further investigated. Brown et al. [84], have performed detailed simulations of convective and shear boundary layers. In general their results are similar to those of [79]. However, they note that in coarsely resolved simulations, the presence of unresolved boundary layers in the flow may require explicit models to account for wall forcing; cf. [79] for further discussion.

4.4 Compressible open cavity flow

The results of the preceding section suggest that there is nothing in principle that prevents the implementation of high-resolution methods in flows with wall boundaries (probably apart from the need for finer grid resolution in the vicinity of these boundaries). The resolution is always problem dependent but the use of high resolution methods can offer better stability and accuracy in coarsely resolved turbulent flows even when no turbulence model is employed. Further investigation of high-resolution methods in turbulent wall-bounded compressible flows has been conducted in [85, 86]. Two-dimensional LES computations have been carried out for compressible, turbulent flow over an open cavity using hybrid scheme [87]. The hybrid scheme combines a Riemann solver [88, 89] and the flux vector splitting scheme of [90]. The hybrid scheme essentially follows a flux formulation similar to (26). The numerical dissipation is adjusted through flux limiters. According to the flux formulation, the most dissipative scheme (flux vector splitting) carries more weight in very high speed flows

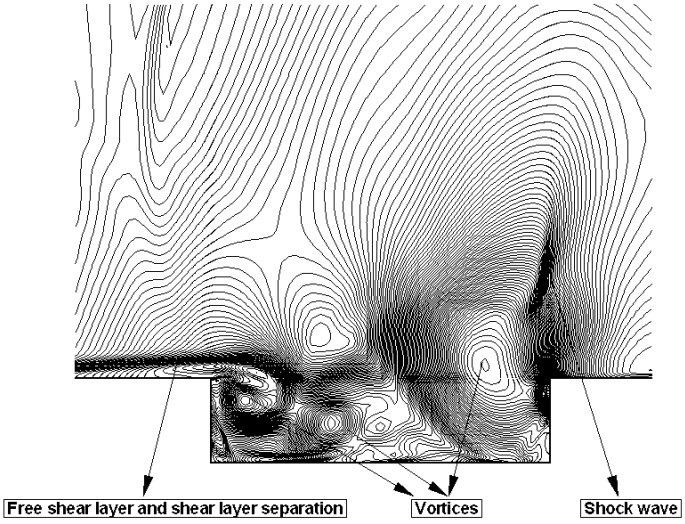

Figure 5: Instantaneous snapshot from two-dimensional embedded LES computations [85, 86] of compressible and turbulent open cavity flow.

(hypersonic flows) in the vicinity of discontinuities where more dissipation is required to ensure stable converged solutions. Investigation of other hybrid formulations for turbulent flows, e.g., using the HLLC scheme of Toro et al. [91] is underway.

In the context of computational aerodynamics pertaining to unsteady flows, the challenge is the achievement of high numerical accuracy in under-resolved - grid-size bias - simulations. At present, in an industrial environment under-resolved simulations are the only alternative for obtaining results in short turnaround times. In order to successfully compute the compressible, turbulent flow in such a geometry, one needs to accurately capture various phenomena including large and small vortical structures; free shear layers; transitional flow, flow separation and flow re-laminarisation; shock and rarefaction waves. Some of these phenomena are shown in Figure 5.

The induced oscillatory pressure field emanating from the cavity geometry are dependent upon the features of the problem. For example, the geometry dimensions,

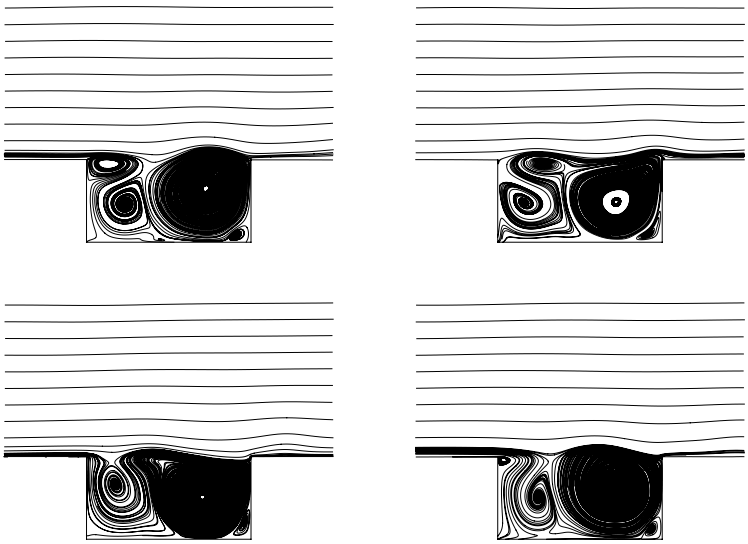

Figure 6: Instantaneous streamlines from the turbulent and compressible cavity $L/D = 2$ flow computations [85, 86].

inflow boundary layer, freestream velocity, etc. Previous numerical investigations of the open rectangular cavity geometry can be divided into either RANS- [92, 93, 94, 95] or DNS-based computations [96, 97]. The RANS investigation of [94], highlighted the fact that accurate predictions of mean pressure, shear layer impingement (onto the rear face of the cavity) and the oscillating pressure field proved arduous without the turbulent shear layer being accurately represented. Nichols et al. [95] employed a RANS approach coupled with $k - \epsilon$ turbulence modelling for open cavity flow fields, expressing, however, concerns regarding the validity of using RANS for such a problem. Traditional Reynolds-stress modelling (time-averaged), when applied to unsteady flows need turbulent timescales, which are diminutive compared to convective timescales.

Cavity flow fields are characterised by such phenomena as unsteady boundary layer separation, instabilities within the shear layer and dominant acoustic flow oscillations. Increasing the length of the cavity, relative to the boundary layer thickness, precipitates the transition of the flow between the shear layer mode and the wake

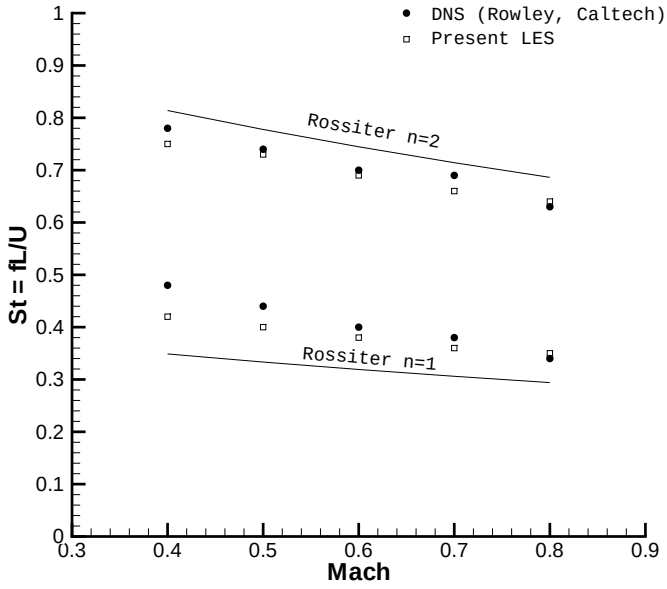

Figure 7: Strouhal number comparison between present (2D) embedded LES, DNS [97] and Rossiter's formula [99].

mode (see [98] for more details). An increase in the freestream Mach number also induces the "switching" of modes. In their experimental study, Gharib and Roshko [98] highlighted the fundamental differences between the shear layer mode and the wake mode. Regarding the difference in the acoustic field of the two modes, they observed that the shear-layer mode occurrs at the downstream cavity edge, and is subjugated by a single frequency (Rossiter Mode II) [99]. Conversely, the field pertaining to the wake mode consists of a number of frequencies and proved to be quite multifaceted. The experiments of [98], determined that the switching between shear and wake modes was a function of the Mach number, and, indeed, this is reinforced in the DNS study of [97].

In [96, 97] DNS was carried out to investigate the resonant instabilities in the flow past an open rectangular cavity at relatively low Reynolds numbers, e.g., $Re = 2,500$ based on the cavity depth. The simulations were performed on a two dimensional

rectangular cavity using approximately $500,000$ grid points. We have carried out 2D LES computations [85, 86] using a grid that is comprised of 283×83 (upper block) and 123×75 (lower block) grid points; the total number of grid points is $32,714$ grid points, i.e., about 15 times less than the number of grid points used in the DNS of [97]. Grid clustering was used around the cavity wall. The distance between the first grid point and the wall was of the order 10^{-4}. The clustering of the grid, especially at the upstream and downstream cavity leading and trailing edges are significant as it is at these points where such phenomena as shear layer formation, shear layer separation and vortex ejection (to name but a few) occur. In the results shown below [86], the length/depth ratio, L/D of the cavity geometry is 2. Simulations for cavity ratios of $L/D = 4$ were also conducted in [85]. The computational domain extends to approximately 5D and 7D upstream and downstream of the cavity leading and trailing edges, respectively. The domain also extends to approximately 9D in the direction normal to the flow. The domain is similar to that of [97]. The flow conditions were Mach number, $M_\infty = 0.8$, and Reynolds number, $Re = 2,500$ (based upon cavity depth, D). For these computations, the instantaneous streamlines at different time instants are shown in Figure 6. Most importantly, Figure 7 shows a very good agreement, for the prediction of the Strouhal number at different Mach numbers, between the 2D embedded LES, the 2D DNS of [97] and Rossiter's semi-empirical formula[6] [99]. Simulations using a SGS (Smagorinsky-type) model have shown no further improvement of the results. This confirms the conclusion of [23] that when no explicit SGS is added a high-resolution method will not add any unnecessary diffusion.

[6]The semi-empirical formula devised by Rossiter [99] defines the resonant frequency by $f = U(m-\gamma)/[L(M_\infty + 1/K)]$, where U is the flow velocity; L is the length of the cavity; K is the ratio of the convective velocity of the shedded vortices to the free stream velocity. The resonant frequency, f, is that of induced unsteady pressure fluctuations. The relationship of $(m-\gamma)$ predicts the sequence of the peaks of highest frequency, which is used to identify the Rossiter's modes [99].

4.5 Shock-bubble interaction

We demonstrate below the dependence of simulations on the high-resolution method using as an example the interaction of a planar shock wave with a cylindrical bubble. Experiments for this problem have been presented in [100] while there have also been various computational studies on the basis of these experiments [30, 101, 102]. Figure 8 shows (instantaneous) isodensity contours as obtained by different Riemann solvers while Fig. 9 presents comparisons between simulations and experiment [25, 103].

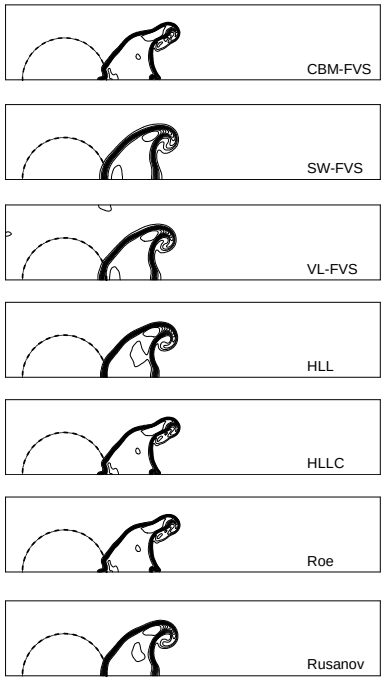

Figure 8: Isodensity contours for the interaction of a shock wave with a dense bubble (R22) as obtained by different high resolution methods. Reproduced with kind permission of Kluwer Academic Publishers, book *"Turbulent Flow Computation"*, 2002, Chapter 2 (pp. 43-74), "High-resolution methods for computing turbulent flows", by W.J. Rider and D. Drikakis, Fig. 2.6 (page 51), D. Drikakis & B.J. Geurts (eds.), ©2002, Kluwer Academic Publishers (printed in the Netherlands) [25].

The results reported below should be considered by bearing in mind the uncer-

tainties associated with the numerical modelling. In the case of the present *inviscid* solution, the shrinking/disappearance of the bubble material is due entirely to numerical diffusion. Therefore, a direct comparison between such simulations and real-world effects of molecular diffusion and turbulent mixing should be considered with extreme prudence. Although one can argue that uncertainties arising from numerical diffusion make difficult a direct comparison between such simulations and experiment, the results of Figs. 8 and 9 suggest the following: i) the details of the simulated flow depend on the numerical scheme employed; ii) there are strong similarities between the predictions of certain methods, e.g. the solutions obtained by the hybrid CBM-FVS [87], HLLC [91] and Roe [105] schemes show stronger similarities than the solutions obtained by the (modified) SW-FVS [87], VL-FVS [48], HLL [106] and Rusanov [107] schemes; iii) even though the solutions obtained by the former group of methods are clearly less diffusive than those obtained by the second group, all schemes provide very similar results for the position of the upstream and downstream bubble interface and also in close agreement with the experiment Fig. 9, at least at the given grid resolution: for a grid containing 500×100 cells, the results obtained by different high resolution schemes differ in absolute value about 0.7% and are therefore indistinguishable on the plot of Fig. 9.

5 Relation of numerics with the physics of turbulent flow and its models

In [22] (see [25] for further discussion) some observations regarding similarities of physical theories, turbulence models (in the context of LES) and numerics were made. This stimulates further investigation of the relation of numerical methods for hyperbolic conservation laws and the physics of turbulent flows (see also [26]). We discuss below various facets of the problem.

The Kolmogorov spectrum [108, 109, 110] describes how the energy density of turbulent structures decreases rapidly with increasing the wave number, where the

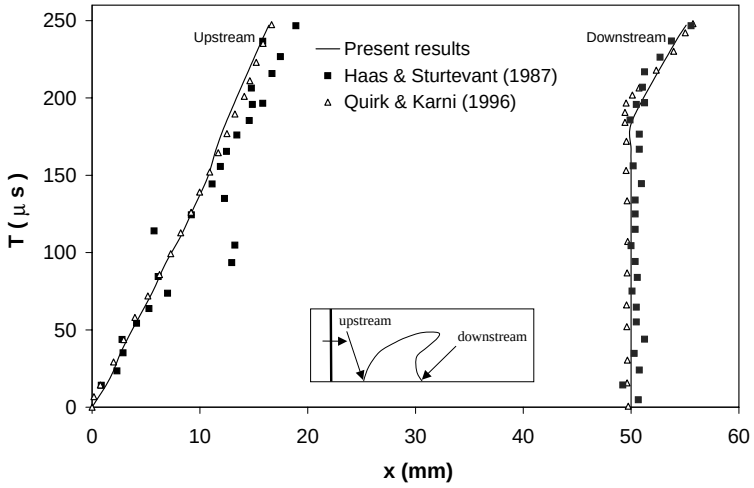

Figure 9: $x-t$ diagram for the interaction of a shock wave $M_s = 1.22$ with a dense bubble; comparison with the experimental results of [100] and adaptive-grid high fidelity simulations of [102]. Reproduced with kind permission of Kluwer Academic Publishers, book *"Turbulent Flow Computation"*, 2002, Chapter 2 (pp. 43-74), "High-resolution methods for computing turbulent flows", by W.J. Rider and D. Drikakis, Fig. 2.7 (page 52), D. Drikakis & B.J. Geurts (eds.), ©2002, Kluwer Academic Publishers (printed in the Netherlands), [25].

Kolmogorov scale is the scale at which the viscous dissipation dominates the inertial flow of the fluid. The downward transfer of energy from large to small scales is called the turbulent cascade process. The latter stops at the Kolmogorov scale, where an eddy is so small that it diffuses rapidly.

Kolmogorov [108, 109] defined a dissipation of kinetic energy that was independent of the coefficient of viscosity in the limit of infinite Reynolds number; this theory was refined in [110]. In this form, the average time-rate-of-change of dissipation of kinetic energy, K, is given as

$$\langle K_t \rangle l = \frac{5}{4} \langle (\Delta u)^3 \rangle \ . \tag{30}$$

In homogeneous, isotropic turbulence, this term is proportional to the average velocity difference at a length scale,l, cubed. Note that this theory is analytic and independent of viscosity. Moreover, this theory provides a basis for the functional form of nonlinear

eddy viscosity, i.e., [54].

Previous computations, experiments and theoretical analysis (see e.g. [63]) has shown that the physics of the turbulent cascade is controlled by the macroscopic scales of the flow and the process of dissipation of this energy due to molecular viscosity takes place primarily at scales considerably larger than the Kolmogorov scale. Another important issue is that the energy transfer is dominated by local interactions. In other words, the energy does not skip from the large to the small scales, but the energy extraction from a given scale occurs as a result of interactions with eddies no more than an order of magnitude smaller.

Bethe [111] derived the dissipation rate due to the passage of a shock wave (for further discussion see [112]). This rate depends on the curvature of the isentrope, $\mathcal{G}$, and on the cube of the jump of dependent variables across the shock:

$$T\Delta S = \frac{\mathcal{G}\rho^3 c^2}{6} (\Delta V)^3 , \tag{31}$$

where ρ is the density and c is the sound speed. Bethe defined this jump in terms of specific volume, V, but this can be restated in terms of velocity by applying the Rankine-Hugoniot conditions, $c\Delta V = -\Delta u$, where s is the shock speed. Both (30) and (31) are analytic results.

For Burgers' equation a similar result may be obtained [113, 114],

$$\langle K_t \rangle \mathcal{L} = \frac{1}{12} \langle (\Delta u)^3 \rangle . \tag{32}$$

Again, this is an analytic result through the application of integration by parts, and the shock jump conditions. In a sense (32) is an entropy condition for Burgers' turbulence describing the minimum integral amount of inviscid dissipation for a physically meaningful solution. This dissipation is produced at the shocks and is a consequence of and proportional to the jump in dependent variables.

Eyink [115] also studied a conjecture by Kraichnan that the dissipation of kinetic energy as defined by the Kolmogorov similarity is both local as well as integral in nature (by definition, the shock dissipation is local). This regularization is the essence of the physical conditions that numerical methods must reproduce correctly. It is this

idea, viz., the existence of a finite rate of dissipation independent of viscosity with an inherently local nature, that numerical methods can reproduce.

High-resolution methods for hyperbolic conservation laws have been developed to capture with high accuracy the variation of flow and thermodynamic variables occurring across shock waves and other discontinuities. In a sense, these methods aim to correctly reproduce (31). On the basis of the similarity of (30) and (31) one can argue that high-resolution methods can also capture accurately the turbulent cascade as described by (30). We note that the importance of designing methods with exact local conservation with proper entropy production is founded upon the Lax-Wendroff theorem ([37]). This theorem states that if one has a method in discrete conservation form and it converges, it converges to a weak solution. The entropy condition is necessary to choose the physically meaningful weak solution among the infinite set of possible weak solutions.

Further to the above arguments, there is a close connection of the differential forms used in the von Neumann-Richtmyer artificial viscosity [116] and the Smagorinsky eddy viscosity [54, 117] often used in LES. It is often noted that Smagorinsky viscosity simplifies to von Neumann-Richtmyer in one dimension. The gradient of the von Neumann-Richtmyer artificial viscosity that is added to the momentum equation has the one-dimensional form

$$\frac{\partial \sigma}{\partial x} = \frac{\partial}{\partial x}\left[-c(\Delta x)^2 \frac{\partial u}{\partial x}\left|\frac{\partial u}{\partial x}\right|\right], \tag{33}$$

where c is a constant and Δx is the grid spacing. The Smagorinsky model for the SGS "stress" in one dimension leads to a very similar relation

$$\frac{\partial \sigma}{\partial x} = \frac{\partial}{\partial x}\left[-c_s \frac{\partial u}{\partial x}\left|\frac{\partial u}{\partial x}\right|\right]. \tag{34}$$

where c_s is the Smagorinsky constant. Indeed, this connection is more explicit than is commonly appreciated, as the original motivation for Smagorinsky's viscosity was to use a nonlinear von Neumann-Richtmyer viscosity to stabilize calculations [117]. These two forms of dissipation differ mainly in the detailed form of their nonlinear

terms in multiple dimensions. Since its conception the von Neumann-Richtmyer viscosity has become significantly more sophisticated, e.g. [118]. Other developments are detailed in [119] including limiters that turn a viscosity off should the flowfield be considered resolved by the numerical derivatives.

The multidimensional extension of von Neumann viscosity was done isotropically by Smagorinsky. In general, the nonlinear viscosity resulting from artificial viscosity or high resolution methods is anisotropic. Isotropic models for artificial viscosity do however exist [119]. Typically, this anisotropic viscosity is proportional to the gradient of the normal velocity in the direction chosen. The general nature of this formalism itself distinguishes this nonlinear viscosity from the typically applied modelling approach. Other types of viscosity are patterned after physical Navier-Stokes viscosity having an isotropic multidimensional form or are rotated into the frame of a shock much like rotated Riemann solvers.

Further similarities exist with the form of the third-order terms found in the Camassa-Holm equations [120]. Because the Camassa-Holm equations imply a dissipation that results from time-averaging determined by dynamical theory, there is a strong connection between the entropy production and the proper nonlinear dissipative form. Such observations suggest that these numerical methods as well as turbulence models all share common dynamical mechanisms for producing entropy.

Modern high-resolution methods have an effective subgrid model that is inherently local. In addition, the algebraic form of the high resolution methods has a great deal in common with scale-similarity forms of LES subgrid models coupled with a nonlinear eddy viscosity. This creates a coherent link between the modern high resolution shock capturing methods and LES subgrid models.

The theory for numerical methods for hyperbolic conservation laws, albeit in one dimension, is quite well developed. In [112] the connection between a thermodynamically consistent equation of state and hyperbolic wave structure is elucidated. This follows the mathematical description due to Lax [121, 122] leading to the current numerical theory and analysis [49]. This combination has culminated with the availability of powerful numerical methods for several decades pervading many application

areas in physics and engineering. Open questions still exist in two or three dimensions, for example: are some multidimensional well-posed, i.e., stable [123]. It has been shown [124, 125] that the case where the solution involves a vortex sheet, the solution to the two-dimensional Riemann problem shows a progression of greater and greater complexity as the mesh is refined.

6 Concluding Remarks

The use of high-resolution methods as an implicit way to model and compute turbulent flows is indeed an evolving area of research. The success of these methods to compute turbulent flows without need to resort to an explicit turbulence model has been proven by a number of studies in the literature and, additionally, there are recent efforts aiming at a rigorous theoretical justification [22, 26].

The desire for understanding better the physics encompassed by numerical methods, high-resolution methods in particular, is motivated by the fact that almost all practical computations in engineering are under-resolved. Numerical aspects play an important role in turbulent-flow computations in terms of both accuracy and efficiency. Numerical methods encompass numerical dissipation which acts to regularize the flow, thereby allowing shock propagation to be captured physically realistically even if it is not fully resolved on the computational mesh. One develops numerical schemes with two competing criteria in mind: a desire for high accuracy coupled with protections against catastrophic failure due to nonlinear wave steepening or unresolved features. Nonlinear mechanisms (limiters) in high-resolution methods guard the methods from such catastrophic failures by triggering entropy producing mechanisms that safeguard the calculation when the need arises. The two key questions are: (i) what criteria should be used to design the nonlinear mechanism that triggers the entropy production, and (ii) to what extent numerical dissipation accounts for turbulent flow effects. Ideally, we would like to quantify the numerical dissipation that is added to computations.

The theory of numerical methods for hyperbolic conservation laws has made sig-

nificant progress in one-space dimension. However, we need to further understand the nonlinear behaviour of numerical methods in multi-dimensional problems. This nonlinear behaviour is also closely related to the numerical mechanisms underlying the formation of spurious solutions in under-resolved flows [124]. Previous studies [124, 125, 126] seem to indicate that the generation of spurious vortices in under-resolved simulations depends solely on the advective scheme. In particular, it depends strongly on how the numerical dissipation is partitioned between different terms of the advective scheme. Although one can succeed to regain control over deficient (spurious-wise) schemes [124, 125] by modifying the dissipative terms of the schemes the exact numerical mechanism is not yet understood. In particular, the question "why certain schemes evince spurious solutions while others do not" still eludes a scholastic answer. In [124] it was shown that for an idealized finite-difference scheme the definition of the advective velocities in the primitive variable formulation of the equations can induce a truncation error vorticity source. However, a rigorous vorticity analysis of nonlinear approximations such as high-order Godunov-type schemes appears very difficult.

The success of high-resolution methods to compute turbulent flows as well as the issue of spurious solutions in under-resolved flows seem to depend on a delicate balance of truncation errors due to wave-speed-dependent terms (chiefly responsible for numerical dissipation) in the case of Godunov-type fluxes and hyperbolic part of the flux. It is the essence of this balance that needs to be understood.

Results from the implementation of high-resolution methods in near wall-bounded flows show that in principle there is nothing that prevents the use of the methods in near wall flows even without using an explicit turbulence model. However, further validation in near wall turbulent flows is required. We note that LES based on an explicit turbulence model also poses substantial challenges in high-Reynolds near-wall flows, especially in the presence of separation from gently curved surfaces, where resolution and thus computing-cost issues are critical.

Acknowledgements:

The author is grateful to Piotr Smolarkiewicz and Joseph Prusa for their kind permission to include figures 3 and 4 in this review. Special thanks go to William Rider and Piotr Smolarkiewicz for various communications on the subject, as well as to Daniela Vassileva and Ahmed Bagabir for their contribution to the cavity flow and shock-bubble interaction computations, respectively. Stimulating discussions with Sergei Godunov, Eleuterio Toro and Randall LeVeque are gratefully acknowledged. The author also acknowledges partial financial support from BAE SYSTEMS and the Isaac Newton Institute for Mathematical Sciences (Cambridge University).

References

[1] Moin P, Kim J. Tackling turbulence with supercomputers. Scientific American 1997; 276: 62-68.

[2] Leschziner MA, Drikakis D. Turbulence and turbulent-flow computation in aeronautics. The Aeronautical Journal. 2002; Paper No 2729 (July 2002): 349-384.

[3] Leschziner MA. Turbulence modelling for separated flows with anisotropy-resolving closures. Phil Trans. Royal Society, Series A 2000: 358: 3247-77.

[4] Barakos G, Drikakis D. Unsteady separated flows over manoeuvering lifting surfaces. Phil. Trans. Royal Soc. Lond. A 2000; 358: 3279-91.

[5] Barakos G, Drikakis D. Computational study of unsteady flows around oscillating and ramping aerofoils. International Journal for Numerical Methods in Fluids 2003: 42(2), 163-86.

[6] Drikakis D, Durst F. Investigation of flux formulae in shock wave turbulent boundary layer interaction. International Journal for Numerical Methods in Fluids 1994; 18: 385-413.

[7] Doyle Knight D., Panaras AG, Yan H, Zheltovodov A. Advances in CFD prediction of shockwave turbulent boundary layer interactions. Progress in Aerospace Sciences 2003; 39: 121-84.

[8] Ghosal S, Moin P. The basic equations for the large eddy simulation of turbulent flows in complex geometry. J. Comput. Phys. 1995; 118: 24-37.

[9] Fureby C, Tabor G. Mathematical and physical constraints of large eddy simulations. 1997; J. Theor. Comp. Fluid Dyn. 9: 85-102.

[10] Ghosal S. Analysis and control of errors in the numerical simulation of turbulence. In: Turbulent Flow Computation, Kluwer Academic Publishers (eds. D. Drikakis, B.J. Geurts), 101-140, (2002).

[11] Van der Ven H. A family of large eddy simulation filters with nonuniform filter widths. Phys. Fluids 1995; 7(5): 1171-1172.

[12] Vasilyev OV, Lund TS, Moin P. A general class of commutative filters for LES in complex geometries. J. Comput. Phys. 1998; 146(1): 82-104.

[13] Vreman B, Geurts B, Kuerten H. Discretization error dominance over subgrid terms in large eddy simulation of compressible shear layers in 2D. Int. J. Numer. Meth. in Engrg. 1994; 10: 785–90.

[14] Phillips NA. An example of nonlinear computational instability. In: the Atmosphere and Sea in Motion (ed. B. Bolin), Rockefeller Inst. Press, New York 1959.

[15] Geurts BJ, Froelich J. A framework for predicting accuracy limitations in large eddy simulations. Phys. Fluids 2002; 14(6): 41-44.

[16] Oran ES, Boris JP. *Numerical Simulation of Reactive Flow*, Elsevier, 2001.

[17] Boris JP, Grinstein FF, Oran ES, Kolbe RJ. New insights into large eddy simulation. Fluid Dyn. Res. 1992; 10: 199-228.

[18] Fureby C, Grinstein FF. Monotonically integrated large eddy simulation of free shear flows. 1999; AIAA J. 37: 544-557.

[19] Fureby C, Grinstein FF. Large eddy simulation of high Reynolds number free and wall bounded flows. J. Comput. Phys. 2002; 181: 68-97.

[20] Porter DH, Pouquet A, Woodward PR. Kolmogorov-like spectra in decaying three-dimensional supersonic flows. Phys. Fluids 1994; 6: 2133-42.

[21] Porter DH, Pouquet A, Woodward PR. Three-dimensional supersonic homogeneous turbulence: A numerical study. Phys. Rev. Lett. 1992; 68: 3156-3159.

[22] Margolin LG, Rider WJ. A Rationale for Implicit Turbulence Modeling. Int. J. Numer. Meth. Fluids 2001; 39: 821-841.

[23] Margolin LG, Smolarkiewicz PK, Sorbjan Z. Large eddy simulations of convective boundary layers using nonoscillatory differencing. Physica D 1998; 133:390–97.

[24] Drikakis D. Embedded turbulence model in numerical methods for hyperbolic conservation laws. Int. J. Numer. Meth. Fluids 2002; 39:763-81.

[25] Rider WJ, Drikakis D. High resolution methods for computing turbulent flows. In: Turbulent Flow Computation, Kluwer Academic Publishers (eds. D. Drikakis, B.J. Geurts), 43-74, (2002).

[26] Rider WJ, Margolin LG. From numerical analysis to implicit subgrid turbulence modeling. AIAA Paper 2003-4101, 2003.

[27] Hirsch C. Numerical Computation of Internal and External Flows. John Wiley and Sons, New York, 1999.

[28] Pope SB. Turbulent Flows, Cambridge University Press, Cambridge, 2000.

[29] Sagaut P. Large eddy simulation for incompressible flows. Springer Verlag, Heidelberg, 2001.

[30] Bagabir A, Drikakis D. Mach number effects on shock-bubble interaction. Shock Waves J. 2001; 11:209-18.

[31] Toro EF. Riemann Solvers and Numerical Methods for Fluid Dynamics: A Practical Introduction, Springer-Verlag, 1997.

[32] Drikakis D, Rider WJ. High-Resolution Methods for Incompressible Flows. Springer Verlag, 2003, in preparation.

[33] Harten A. High resolution schemes for hyperbolic conservation laws. J. Comput. Phys. 1983; 49:357–93.

[34] Harten A, Engquist B, Osher S, Chakravarthy S. Uniformly high order accurate essentially non-oscillatory schemes III. J. Comp. Phys. 1987; 71: 231–303.

[35] Godunov SK. Finite Difference Method for Numerical Computation of Discontinuous Solutions of the Equations of Fluid Dynamics. Matematicheski Sbornik 1959; 47:271–306.

[36] Godunov SK., private communication, (unpublished numerical experiments) 2003.

[37] Lax PD, Wendroff B. Systems of conservation laws. Communications in Pure and Applied Mathematics 1960; 13:217–37.

[38] Roe PL. Numerical algorithms for the linear wave equation. Technical Report 81047, Royal Aircraft Establishment, Bedford, UK, 1981.

[39] Roe PL. Some contribution to the modelling of discontinous flows. In: Proceedings of the SIAM/AMS Seminar, San Diego, 1983.

[40] Boris JP, Book DL. Flux-corrected transport III: Minimal-error FCT algorithms. J. Comput. Phys. 1976; 20: 397-431.

[41] Sweby PK. High resolution schemes using flux limiters for hyperbolic conservation laws. SIAM J. Num. Anal. 1984; 21:995–1011.

[42] Boris JP, Book DL. Flux-corrected transport. I. A fluid transport algorithm that works. J. Comput. Phys. 1973; 11: 38-69.

[43] Van Leer B. Towards the ultimate conservative difference scheme. II. Monotonicity and conservation combined in a second-order scheme. J. Comput. Phys. 1974; 14: 361-370.

[44] Van Leer B. Towards the ultimate conservative difference scheme. III. Upstream-centered finite difference schemes for ideal compressible flow. J. Comput. Phys. 1977; 23: 263-275.

[45] Van Leer B. Towards the ultimate conservative difference scheme. IV. A second order sequel to Godunov's method. J. Comput. Phys. 1977; 23: 276-299.

[46] Van Leer B. Towards the ultimate conservative difference scheme. V. A new approach to numerical convection. J. Comput. Phys. 1979; 32: 101-136.

[47] Van Albada GD, Van Leer B, Roberts WW. A comparative study of computational methods in cosmic gas dynamics. Astron. Astrophysics 1982; 108: 76–84.

[48] Thomas JL, van Leer B, Walters RW. Implicit flux split scheme for the Euler equations. AIAA-Paper 85-1680, 1985.

[49] Leveque RJ. Finite Volume Methods for Hyperbolic Problems. Cambridge Univ. Press, 2002.

[50] Thuburn J. TVD schemes, positive schemes, and the universal limiter. Monthly Weather Review 1990; 125: 1990-93.

[51] Hundsdorfer W, Koren B, van Loon M, Verwer JG. A positive finite difference advection scheme. Applied Mathematics and Computation 1995; 117: 35-46.

[52] Leonard BP. The ULTIMATE convective difference scheme applied to unsteady one-dimensional advection. Computer Methods in Applied Mechanics & Engnrg 1991; 88: 17-74.

[53] Warming RF, Hyett BJ. The modified equation approach to the stability and accuracy analysis of finite-difference methods. J. Comput. Phys. 1974; 14:159-79.

[54] Smagorinsky J. General circulation experiments with the primitive equations. I. the basic experiment. Mon. Wea. Rev. 1963; 101: 99–164.

[55] Anderson W, Thomas JL, Van Leer B. Comparison of finite volume flux vector splittings for the Euler equations. AIAA Journal 1986; 24: 1453-60.

[56] Lilly DK. A proposed modification of the Germano subgrid-scale closure method. Phys. Fluids 1992; 4: 633-35.

[57] Germano M, Piomelli U, Moin P, Cabot WH. A dynamic subgrid-scale eddy viscosity model. Phys. Fluids 1991; 3(7): 1760-65.

[58] Smolarkiewicz PK, Margolin LG. MPDATA: a finite difference solver for geophysical flows. J. Comput. Phys. 1998; 140:459–80.

[59] Lax PD. Weak solutions of nonlinear hyperbolic equations and their numerical computation. Comm. Pure Appl. Math. 1954; VII: 159-93.

[60] Hirt CW. Heuristic stability theory for finite difference equations. J. Comput. Phys. 1968; 2:339-355.

[61] Harten A, Hyman JM, Lax PD. On finite difference approximations and entropy conditions for shocks. Communications on Pure and Applied Mathematics 1976; 29:297-322.

[62] Rider WJ, Margolin LG, Kamm JR. Techniques for the analysis of nonlinear approximations to nonlinear equations. Manuscript LA-UR-02-3215, Los Alamos National Laboratories, 2002.

[63] Oran ES, Boris JP. Computing turbulent shear flows – A convenient conspiracy. Computers in Physics 1993; 7(3): 523-33.

[64] Boris JP. In: Whither Turbulence? Turbulence at the Crossroads, J. L. Lumley (ed.), Springer-Verlag, Berlin, 1989.

[65] Grinstein FF. Vortex dynamics and entrainment in regular free jets. J. Fluid Mech. 2002; 437: 69-101.

[66] Grinstein FF, DeVore CR. On global instabilities in countercurrent jets. Phys. Fluids 2002; 14: 1095.

[67] Uthuppan J, Aggarwal SK, Grinstein FF. Particle dispersion in a transitional axisymmetric jet: A numerical simulation. AIAA J. 1994; 32(10): 2004-14.

[68] Grinstein FF, Fureby C. Recent progress on MILES for high Reynolds number flows. J. Fluids Engnrg. 2002; 124: 848-861.

[69] Sytine IV, Porter DH, Woodward PR, Hodson SW, Winkler KH. Convergence tests for the piecewise parabolic method and Navier-Stokes solutions for homogeneous compressibble turbulence. J. Comput. Phys. 2000; 225-38.

[70] Woodward PR, Porter DH, Yang W, Mei Q. Simulation and visualisation of compressible convection in 2D and 3D. In Nonlinear Astrophysical Fluid Dynamics, Annals of the New York Academy of Science (New York Acad. Sci., New York 1990), 67, 234.

[71] Garnier E, Mossi M, Sagaut P, Comte P, Deville M. On the use of shock capturing schemes for large eddy simulation. J. Comput. Phys. 2000; 153: 273.

[72] Mallinger B, Drikakis D. Laminar-to-turbulent transition in pulsatile flow through a stenosis. Biorheology Journal 2002; 39: 437-441.

[73] Mallinger B, Drikakis D. Instability in three-dimensional, unsteady stenotic flows. Int. J. Heat and Fluid Flow 2002: 23: 657-663.

[74] Fureby C, Moller S-I. Large eddy simulation of reacting flows applied to bluff body stabilized flames. AIAA J. 1995; 33: 2339.

[75] Drikakis D, Geurts BJ. Turbulent Flow Computation, Kluwer Academic Publishers, 2002.

[76] Kraichnan RH. Lagrangian-history statistical theory for Burgers' equation. Phys. Fluids 1968; 11: 265–77.

[77] Drikakis D. Uniformly high-order methods for unsteady incompressible flows. Godunov Methods: Theory and Applications, Kluwer Academic Publishers (ed. E.F. Toro), 2001, 263-83.

[78] Métais O, Lesieur M. Spectral large-eddy simulations of isotropic and stably-stratified turbulence. J. Fluid Mech. 1992; 239:157-94.

[79] Smolarkiewicz PK, Prusa JM. Forward-in-time differencing for fluids: Simulations of geophysical turbulence. In: Turbulent Flow Computation, Kluwer Academic Publishers (eds. D. Drikakis, B.J. Geurts), 279-312, 2002.

[80] Margolin LG, Smolarkiewicz PK, Wyszogrodzki AA. Implicit turbulence modeling for high Reynolds number flows. J. Fluids Engnrg. 2002; 124: 862-67.

[81] Herring JR, Kerr RM. Development of enstrophy and spectra in numerical turbulence. Phys. Fluids A 1993; 5: 2792-98.

[82] Lesieur M. Turbulence in Fluids. Kluwer Academic Publ. 1997.

[83] Schmidt H, Schumann U. Coherent structure of the convective boundary layer derived from large-eddy simulation. J. Fluid Mech. 1989; 200: 511-562.

[84] Brown AR, MacVean MK, Mason PJ. The effects of numerical dissipation in large eddy simulations. J. Atmos. Sci. 2000; 120: 3337-48.

[85] Drikakis D, Fookeer FA, Vassileva D. Computation of compressible cavity flows using high resolution methods. Proceedings of the CEAS Aerospace Aerodynamics Research Conference, June 2002, Cambridge, UK.

[86] Fookeer F, Drikakis D. Computational challenges for turbulent, compressible open cavity flows. Project report, BAE Systems, 2002.

[87] Zółtak J, Drikakis D. Hybrid upwind methods for the simulation of unsteady shock-wave diffraction over a cylinder. Comput. Meth. Appl. Mech. & Engrg. 1998.; 162: 165-85.

[88] Eberle A. Characteristic flux averaging approach to the solution of Euler's equations. VKI Lecture Series 1987-04, 1987.

[89] Eberle A, Rizzi A, Hirschel EH. Numerical Solutions of the Euler Equations for Steady Flow Problems. Notes on Numerical Fluid Mechanics, 34, Vieweg Verlag, Wiesbaden, 1992.

[90] Drikakis D, Tsangaris S. On the solution of the compressible Navier-Stokes equations using improved flux vector splitting methods. Applied Mathematica Modelling 1993; 17: 283-297.

[91] Toro EF, Spruce M, Speares W. Restoration of the contact surface in the HLL-Riemann solver. Shock Waves J. 1994; 4: 25-34.

[92] Baysal O, Yen GW, Fouladi K. Navier Stokes Computations of Cavity Aeroacoustics with Suppression Devices. AIAA/DLGR Paper 92-02-161, May 1992.

[93] Zhang X. Compressible Cavity Flow Oscillations due to Shear Layer Instabilities and Pressure Feedback. AIAA Journal 1995; 33(8): 1404-11.

[94] Shih SH, Hamed A, Yeuan JJ. Unsteady supersonic cavity flow simulations using coupled $k-\epsilon$ and Navier Stokes Equations. AIAA J. 1996; 32(10): 2015-21.

[95] Nichols RH, Tramel RW. Applications of a highly efficient numerical method for overset-mesh moving body problems. AIAA Paper No. 97-2255, June 1997.

[96] Colonius T, Basu AJ, Rowley CW. Numerical investigation of the flow past a cavity. AIAA Paper 99-1912, 5th AIAA/CEAS Aeroacoustics Conference, Greater Seattle Washington, 10-12 May, 1999.

[97] Rowley CW. Modelling, simulation and control of cavity flow oscillations. PhD Thesis, California Institute of Technology, 2002.

[98] Gharib M, Roshko A. The effect of flow oscillations on cavity drag. J. Fluid Mech. 1987; 177: 501-30.

[99] Rossiter, J.E., "Wind-Tunnel Experiments on the Flow over Rectangular Cavities at Subsonic and Transonic Speeds". British Aeronautical Research Council, Reports and Memoranda No. 3436, Oct. 1964.

[100] Haas JF, Sturtevant B. Interaction of weak shock waves with cylindrical and spherical gas inhomogeneities. J. Fluid Mech. 1987; 181: 41-76.

[101] Picone JM, Boris JP. Vorticity generation by shock propagation through bubbles in a gas. J. Fluid Mech. 1988; 189: 23-51.

[102] Quirk JJ, Karni S. On the dynamics of a shock-bubble interaction. J. Fluid Mech. 1996; 318: 129-63.

[103] Bagabir A. On the accuracy and efficiency of Godunov -type methods in various compressible flows. 2000 *PhD Dissertation*, Queen Mary College, University of London.

[104] Bagabir A, Drikakis D. Performance of Godunov-type methods in time-dependent compressible flows. in preparation 2003.

[105] Roe PL, Pike J. Efficient construction and utilisation of approximate Riemann solutions. In Computing Methods in Applied Science and Engineering, North-Holland, 1984.

[106] Harten A, Lax PD, van Leer B. On upstream differencing and Godunov-type schemes for hyperbolic conservation laws. SIAM Review 1983; 25: 35–61.

[107] Rusanov VV. Calculation of interaction of non-steady shock waves with obstacles. J. Comput. Math. Phys. USSR 1961; 1: 267-79.

[108] Kolmogorov AN. The local structure of turbulence in incompressible viscous fluid at very high Reynolds number. Dokl. Akad. Nauk SSSR 1941; 30:538-41. Reprinted Kolmogorov Anniversary Edition. 1991 Proc. Roy. Soc. Lond., A434.

[109] Kolmogorov AN. Energy decay in locally isotropic turbulence. Dokl. Akad. Nauk SSSR 1941; 31:16-18. Reprinted Kolmogorov Anniversary Edition, 1991 Proc. Roy. Soc. Lond. A434.

[110] Kolmogorov AN. A refinement of previous hypotheses concerning the local structure of turbulence in a viscous incompressible fluid at high Reynolds number. J. Fluid Mech. 1962; 13:82–85.

[111] Bethe HA. On the Theory of Shock Waves for An Arbitrary Equation of State. In *Classic Papers in Shock Compression Science*, J.N. Johnson & R. Cheret (eds.), Springer-Verlag, Berlin, 1998.

[112] Menikoff R, Plohr BJ. The Riemann problem for fluid flow of real materials. Reviews in Modern Physics 1989; 61:75–129.

[113] Bec J, Frisch U, Khanin K. Kicked Burgers' turbulence. J. Fluid Mech. 2000; 416:239–267.

[114] Gurbatov SN, Simdyankin SI, Aurell E, Frisch U, Toth G. On the decay of Burgers' turbulence. J. Fluid Mech. 1997; 344:339–374.

[115] Eyink G. Local energy flux and the refined similarity hypothesis. 1995; J. Stat. Phys. 1995; 78:335–51.

[116] Von Neumann J, Richtmyer RD. A method for the numerical calculation of hydrodynamic shocks. J. Appl. Phys. 1950; 21: 232–237.

[117] Smagorinsky J. The beginnings of numerical weather prediction and general circulation Modeling: Early Recollections. Advances in Geophysics 1983; 25: 3–37.

[118] Caramana EJ, Shashkov MJ, Whalen PP., Formulations of Artificial Viscosity for Multi-Dimensional Shock Wave Computations, J. Comput. Phys. 1998; 144:70–97.

[119] Benson DJ. Computational Methods in Lagrangian and Eulerian Hydrocodes. Computer Methods in Applied Mechanics and Engineering 1992; 99: 235–94

[120] Camassa R, Holm DD. An integrable shallow-water equation with peaked solitons. Phys. Rev. Lett. 1993; 71:1661–64.

[121] Lax PD. Shock waves and entropy. Contributions to Nonlinear Functional Analysis, Academic Press, E. H. Zarantonello (Ed.), 1971, 603–634.

[122] Lax PD. Hyperbolic Systems of Conservation Laws and the Mathematical Theory of Shock Waves, SIAM, Philadelphia, USA, 1972.

[123] Lax PD, Liu X-D. Solution of two-dimensional Riemann problems of gas dynamics by positive schemes. SIAM J. Sci. Comput. 1998; 19(2):319–40.

[124] Drikakis D, Smolarkiewicz PK. On spurious vortical structures. J. Comput. Phys. 2001; 172: 309–325.

[125] Drikakis D, Margolin LG, Smolarkiewicz PK. "Spurious" eddies. International Journal Numerical Methods in Fluids 2002; 40: 313-322.

[126] Yee HC, Sweby PK. Dynamical approach study of spurious steady-state numerical solutions for nonlinear differential equations, Part II: Global asymptotic behavior of time discretizations. Int. J. Comput. Fluid Dyn. 1995; 4: 219-283.